Three-dimensional Fatigue Crack Growth Path Simulation under Non-proportional Mixed-mode Loading

Ying Yang[1,*], Michael Vormwald[1]

[1] Material Mechanics group, Technische Universität Darmstadt, Petersenstaße 12, 64287 Darmstadt (Germany)
* Corresponding author: yang@wm.tu-darmstadt.de

Abstract An algorithm based on linear elastic fracture mechanics (LEFM) for three-dimensional fatigue crack growth simulation under non-proportional mixed-mode loading is proposed in the present paper. Combined non-proportional cyclic tension and torsion loading with different phase angle and loading ratio M_T/F are considered. The maximum tangential stress (MTS) criterion is performed as the main theory to predict crack propagation direction. Under some specific loading cases, especially for high stress intensity factors, the crack growth direction needed to be modified in order to be in accordance with the experimental results. By analyzing the simulated crack growth paths, three distinct features are observed that are tension mode dominated crack paths, shear mode dominated crack paths and transitional crack paths. When crack growth changes from tension to shear mode, the latter is described by the maximum shear stress (MSS) criterion. A preliminary proposal is made to predict the transitional mode.

Keywords Linear elastic fracture mechanics, Non-proportional loading, Mixed mode, Transitional fracture

1. Introduction

Considering that a great amount of structures or components are subjected to mixed mode loading during the service time, research on material fracture under this kind of loading type has attracted more attention in recent years. Crack propagation direction is one of the major problems in this field. Since the maximum tangential stress criterion was first proposed by Erdogan and Sih [1], the minimum strain energy density criterion (S-Criterion), the maximum energy release rate criterion and maximum tangential strain criterion [2–4] and so on were suggested subsequently. All the mentioned criteria present similar crack propagation direction for proportional mixed mode loading, showing small deviation with the experiment results. The crack growth directions display a tension mode feature following the direction which minimizes the K_{II} values. However, large distinction between experimental crack propagation direction and the predicted crack kink angle were also observed for some materials. In these cases, the crack growth occurred in the plane that K_{II} values were maximum. As a result the maximum shear stress (MSS) criterion was proposed. Crack growth in shear mode was summarized in a literature review by H. W. Liu [5].

The criteria represented by MTS and MSS are deduced according to the stress field solution in the vicinity of crack tip on the basis of linear elastic fracture mechanics. Strictly speaking, these criteria are appropriate only in monotonic loading condition. Nevertheless, Highsmith et al. [6] pointed out that the criteria can be performed straightforward to fatigue crack growth under proportional mixed mode loading. Fatigue crack growth under non-proportional mixed mode loading is a more complex situation and there are insufficient experiments and hypotheses for application. Vormwald et al. [7] reviewed some research consequences in recent years. Six relevant factors which influence the crack growth behavior under non-proportional loading were denoted and an algorithm based on LEFM for three-dimensional fatigue crack growth simulation under non-proportional mixed-mode loading is proposed [8]. The emphasis in the present paper is focusing on the crack growth path behavior. A description of the algorithm is presented.

2. Application of the algorithm

The algorithm is applied to simulate the fatigue crack growth including path and propagation rate in a thin-walled, hollow cylindrical specimen (see Figure 1) with a notch. The corresponding experimental data were obtained by Brüning [9]. In the experiment two common used materials were tested, the aluminium alloy AlMg4.5Mn and steel S460N. The combined non-proportional cyclic tension and torsion loading with phase angles of 45° and 90° were applied to the specimens with an R ratio of -1. The results of 4 specimens marked as A7, A8, S7 and S13 could be used here for comparison purpose because the loading was relatively low to meet small scale yielding requirements.

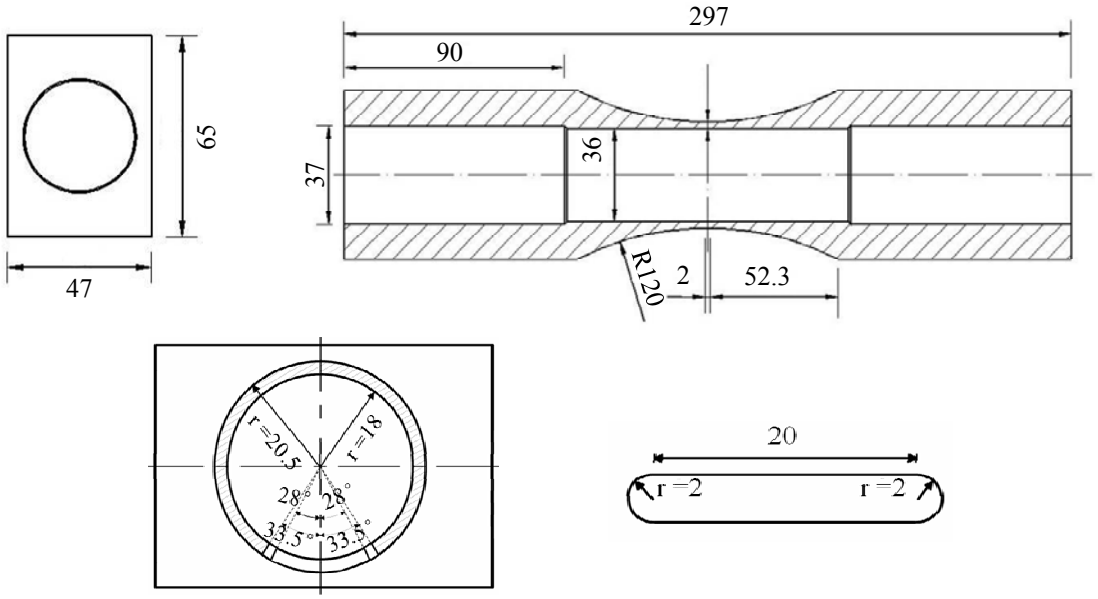

Figure 1. Specimen and notch geometry (dimensions in millimetres)

The algorithm consists of three main modules: (a) determination of the crack initiation position; (b) calculation of the maximum equivalent stress intensity factor K_{eq} in one loading cycle, which is taken as the crack driving force parameter; (c) crack growth process. Module (b) and (c) are repeated until the crack growth path can be presented clearly. Brief expression of each module is introduced in the following sections, more details can be found in reference [8].

2.1. Location of crack initiation

The crack initiation will occur in the notch root at the position where the locally uniaxial notch stress is maximum in one loading cycle. A 3-dimensional finite element model was created using ABAQUS software for stress analysis. Refined mesh was applied in the crack growth region as shown in Fig 2 (a). Along the notch root, there are four potential crack initiation sites numbered 1, 2, 3 and 4 clockwise, shown in Fig 2 (b). The analysis indicated that the maximum tangential stress in one loading cycle along the notch root on the inside edges is almost 2 times larger than the tangential stress on the outside edge, therefore a corner crack is considered to be a reasonable shape to initial crack simulation. As can be expected, the initial corner crack will propagate through the thickness of the notch and extend to the outside surface of the specimen in the crack growth process.

An incipient corner crack was inserted into the inside edge of the notch root where tangential stress is maximum by program Fracture Analysis Code 3D (FRANC3D). This program package is designed to simulate crack growth in engineering structures or components with arbitrary crack

geometry under different loading and boundary conditions. FRANC3D adaptively remeshes an existing finite element model with the inserted initial crack to generate a cracked model. Furthermore, FRANC3D is also used to calculate stress intensity factor (SIF) for an entire crack front.

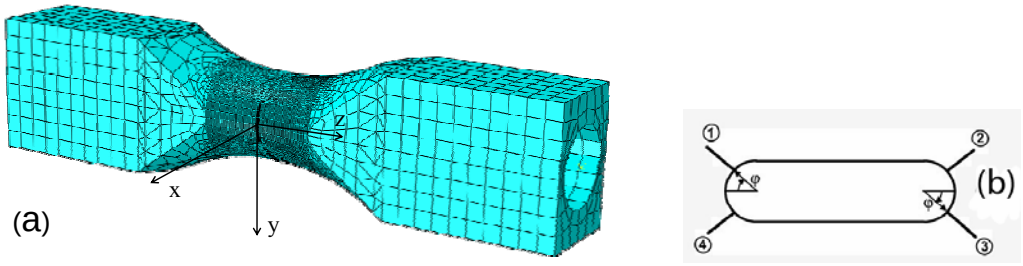

Figure 2. (a) Finite element model, (b) Crack initiation sites

2.2. Crack driving force calculation

In the present paper, mode I and mode II SIFs, K_{I} and K_{II} in one cycle under non-proportional tension combined with torsion loading are computed for the sake of obtaining the equivalent SIF, K_{eq}. Erdogan and Sih proposed that the equivalent stress intensity factor according to the maximum tangential stress criterion can be described by:

$$K_{eq}=\frac{1}{4}\left(3\cos\frac{\theta^{*}}{2}+\cos\frac{3\theta^{*}}{2}\right)K_{\mathrm{I}}-\frac{3}{4}\left(\sin\frac{\theta^{*}}{2}+\sin\frac{3\theta^{*}}{2}\right)K_{\mathrm{II}} \tag{1}$$

θ^{*} is a function of K_{I} and K_{II}, representing the direction where the tangential stress $\sigma_{\theta\theta}$ in the vicinity of the crack tip is maximum. And also the shear stress $\tau_{r\theta}$ vanishs along this direction on the basis of MTS criterion.

$$\theta^{*}=2\arctan\left(\frac{1}{4}\frac{K_{\mathrm{I}}}{K_{\mathrm{II}}}\pm\frac{1}{4}\sqrt{\left(\frac{K_{\mathrm{I}}}{K_{\mathrm{II}}}\right)^{2}+8}\right) \tag{2}$$

The stress intensity factors for mode I and mode II are calculated by FRANC3D software for tension F=1 and torsion M_{T} =1. The combined tension and torsion mixed mode stress intensity factors K_{I} and K_{II} are obtained from the superposition according to equation (3):

$$\begin{aligned}K_{\mathrm{I}}(\mathrm{t})&=K_{\mathrm{I},F}\cdot F(\mathrm{t})+K_{\mathrm{I},M}\cdot M_{T}(\mathrm{t})\\K_{\mathrm{II}}(\mathrm{t})&=K_{\mathrm{II},F}\cdot F(\mathrm{t})+K_{\mathrm{II},M}\cdot M_{T}(\mathrm{t})\end{aligned} \tag{3}$$

The combined SIFs computed from equation (3) are inserted to equation (2) to find the angle θ^{*}, which is put into equation (1). The equivalent stress intensity factor K_{eq} is calculated for a full loading cycle. Among all the equivalent stress intensity factors, the peak value $K_{eq,\max}$ is taken as the crack driving force, which means the loads at this instant $t_{\max}$, $F(t_{\max})$ and $M_{\mathrm{T}}(t_{\max})$ are used for

crack propagation simulation.

2.3. Crack growth process

The load corresponding to the $K_{eq,\max}$, $F(t_{\max})$ and $M_T(t_{\max})$ are applied to the cracked finite element model. Stress analysis is carried out in ABAQUS. The SIF solutions for the cracks are again obtained from FRANC3D based on the stress analysis. Although the solutions for K_I, K_{II} and K_{eq} are already at hand for $t = t_{\max}$, the re-evaluation of this loading case combination can now be used to let the FRANC3D software create the crack propagation increment Δa. The ABAQUS/FRANC3D interface was implemented to perform the crack growth analysis. The finite element modeling and the stress analysis are performed in ABAQUS, FRANC3D is used to calculate crack growth parameters and updates the crack geometry and mesh. This process is continued until the crack has grown to a certain length.

As referred before, on one hand the MTS criterion is used as the rule for estimating crack propagation direction in most cases, on the other hand as will be shown later that under certain loading conditions, the simulated crack growth path deviated from the experimental crack path when the length of the crack is long enough. In order to investigate the crack growth path behavior under these complicated loading cases, a modification is essentially to keep the deviation between experimental results and simulation in an acceptable extent. Due to an extremely inadequate hypothesis about the criterion which is suitable for fatigue crack growth direction prediction under non-proportional mixed mode loading, the modification is implemented manually to adjust the position of newly generated crack front in order to make the simulated crack increment direction coincident with the experimental results. As a result, although the simulated crack growth path is not perfectly identical with the experimental data, a close match is enforced.

3. Results

3.1. AlMg4.5Mn specimens

In the experiment, specimen A7 (amplitude load values: F=8kN; M_T=96Nm) was tested under a non-proportional loading with an out of phase angle of 90°, while specimen A8 (amplitude load values: F=6.5kN; M_T=72Nm) was subjected a loading with a out of phase angle of 45°. The crack growth paths are shown in Figure 3. According to the stress analysis for the uncracked specimen, the local tangential stress along the notch root in site 1 and 3 are approximately 1.6 times larger than the stresses in site 2 and 4, therefore cracks should occur in site 1 and 3. Very curvilinear paths were displayed in specimen A7, furthermore in the experiment, crack branching appeared and then the crack growth path continues nearly perpendicularly to the previous propagation direction. The simulation algorithm at present does not contain a condition for crack branching, only the first curvilinear paths are presented. For specimen A8, the crack propagates along an angle of nearly 45° with the longitudinal axis. After the crack reaches a certain length, it has a tendency to turn into a plane, which is perpendicular to the longitudinal axis.

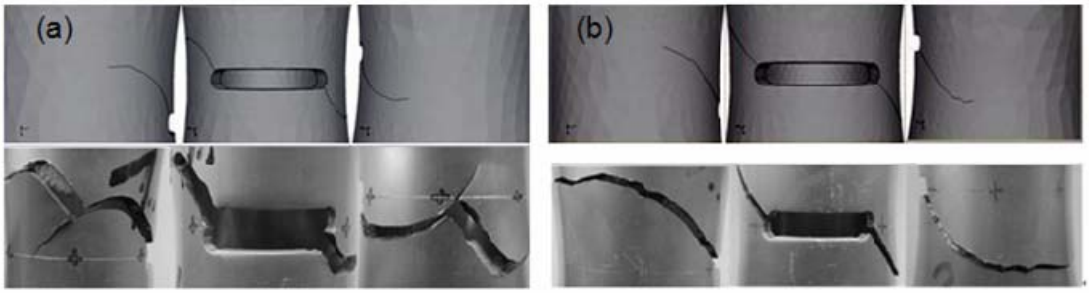

Figure 3. (a)A7 crack growth path, (b) A8 crack growth path [8]

3.2. S460N specimens

Specimen S7 (amplitude load values: F=27kN; M_T=408Nm) under the loading with a out of phase angle of 90° and the corresponding loading phase angle for specimen S13 (amplitude load values: F=22.5kN; M_T=272Nm) is 45°. 4 initial corner cracks are inserted into the notch root in specimen S7 because the maximum local tangential stresses are almost equal for sites 1-4. The crack propagation trend for specimen S13 is similar with specimen A8 as shown in Figure 4(b).

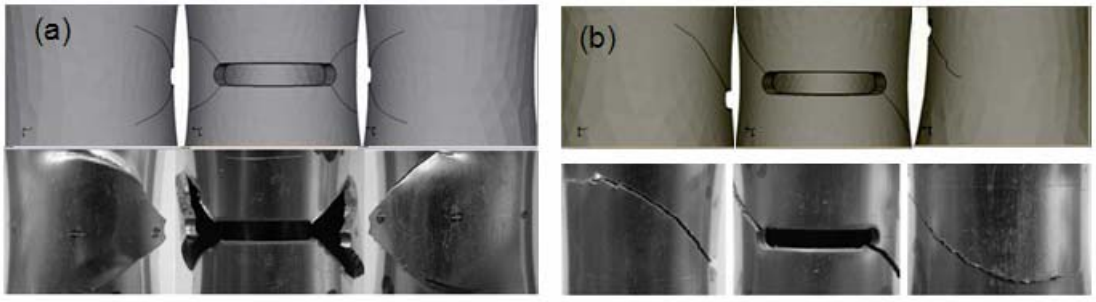

Figure 4. (a) S7 crack growth path, (b) S13 crack growth path [8]

Besides crack growth paths, the fatigue life for each specimen was also calculated based on Paris law. More details and the curves for crack length versus number of cycles are shown in reference [8].

4. Discussion

4.1. Crack propagation behavior of specimen A7

Crack paths are marked as ①, ②, ③ and ④ corresponding to the crack initiation sites as shown in Figure 2(b). The coordinate system is illustrated in Figure 2(a), the centre point of specimen is considered as the origin. The crack propagation trajectory (path ①) for specimen A7 is plotted in Figure 5(a). The solid line represents the simulated crack growth path in FRANC3D. The path labelled by squares is calculated based on the MTS criterion. It can be seen that when the crack reaches to a certain length (the length of this crack is from the notch root to point A), the crack growth path will deviate from the prediction of MTS criterion. From point A, MSS criterion predicted path is marked by triangle symbols. Obviously, the crack path starting from point A does

not follow the route estimated by either MTS criterion or MSS criterion. A path between the prediction of MTS and MSS criteria seems more reasonable compared with the experiment results. From point B, the simulated crack path seems to be controlled by MSS criterion, a negligible deviation can be found in Figure 5(a). In the contrary, large divergence is shown for the crack path estimated by MTS criterion. Based on the LEFM analysis, MTS criterion is valid in tension mode fracture and MSS criterion is used in shear mode problem, both of these two criteria are supported by a large quantity of corresponding experiments. The simulated crack path from point A to point B which keeps the same trend with the experimental result between tensile mode and shear mode is defined as the so called transition mode fracture [10]. Comparing to common investigated tension mode and shear mode, the transition mode is an occasional situation, appearing under very complex and dynamic loading, for instance for the present cyclic non-proportional mixed mode loading.

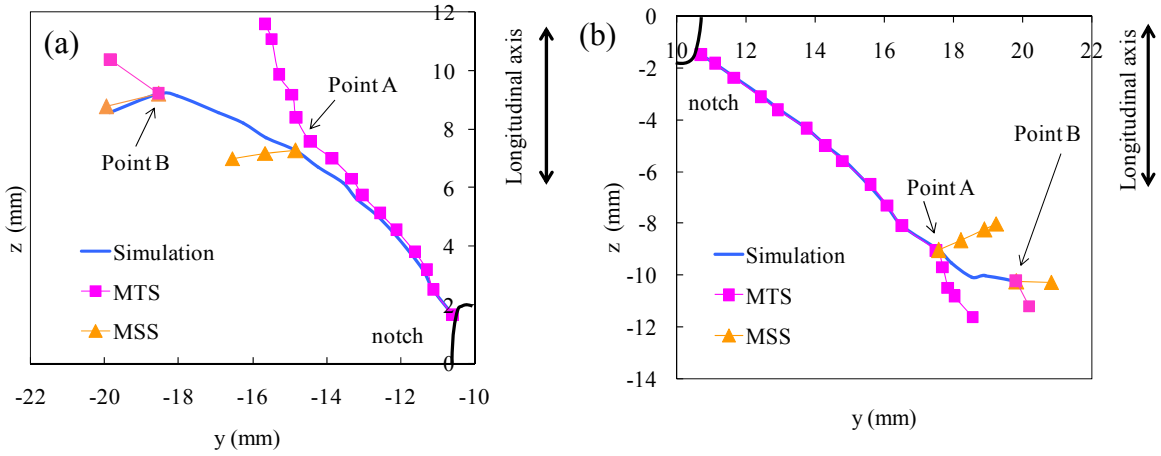

Figure 5. Crack growth path of (a) specimen A7, (b) specimen A8

4.2. Crack propagation behavior of specimen A8

Figure 5(b) shows the propagation crack path ③ for specimen A8. The symbols for different crack growth paths are defined as the same for specimen A7. The crack path starting from the notch root to point A complied perfectly with the prediction of MTS criterion. Beginning with point A, the crack path estimated by MTS criterion propagated almost along with the total previous crack path angle with no obvious transforming for the direction of crack extension. When the MSS criterion predicted crack growth path is contrasted with the MTS one from point A, the difference is very apparent as shown with the triangle diagram in Figure 5(b). The MSS path displayed a sharp deflection with the previous crack path direction and extended nearly in an opposite orientation, which is upward compared to the previous crack path. Obviously, these two crack growth paths do not conform to the experiment result. A path between the prediction of MTS criterion and MSS criterion gradually routed the crack to grow perpendicularly to the longitudinal axial. A transition fracture mode occurred in this specimen. As well as specimen A7, the transition fracture mode is followed by a shear fracture dominant crack path from point B. The MSS criterion predicted crack path could be considered to be perpendicular to the longitudinal axial of specimen. As can be seen from Figure 3(b), in the experiment once the crack changed propagating direction normal to the longitudinal axial, the coplanar shear crack growth is persistent until to the final fracture.

4.3. Crack propagation behavior of specimen S13 and S7

The crack growth path (path ①) for specimen S13 is plotted in Figure 6(a). An acceptable crack path compared with the experimental result from the notch root to point A was predicted by the MTS criterion. The transition fracture mode is expected following tension mode fracture. The simulated crack growth path for this specimen is not long enough to show a complete transition path. Nevertheless, it could be inferred that a shear mode fracture would occur as well as in specimen A8. The crack propagation path of specimen S13 is similar with specimen A8 (see Figure 3(b), Figure 4(b)), the final fracture is a coplanar crack extension perpendicular to the longitudinal axis which can be predicted by MSS criterion. Figure 6(b) illustrates one crack growth path (path ①) for specimen S7. It is found that the presented crack path has good agreement with the predicted crack path using MTS criterion. From the experimental result as shown in Figure 4(a), the crack growth paths did not deflect to the plane perpendicular to the longitudinal axis for coplanar shear crack extension, which means no shear mode fracture occurred in this specimen.

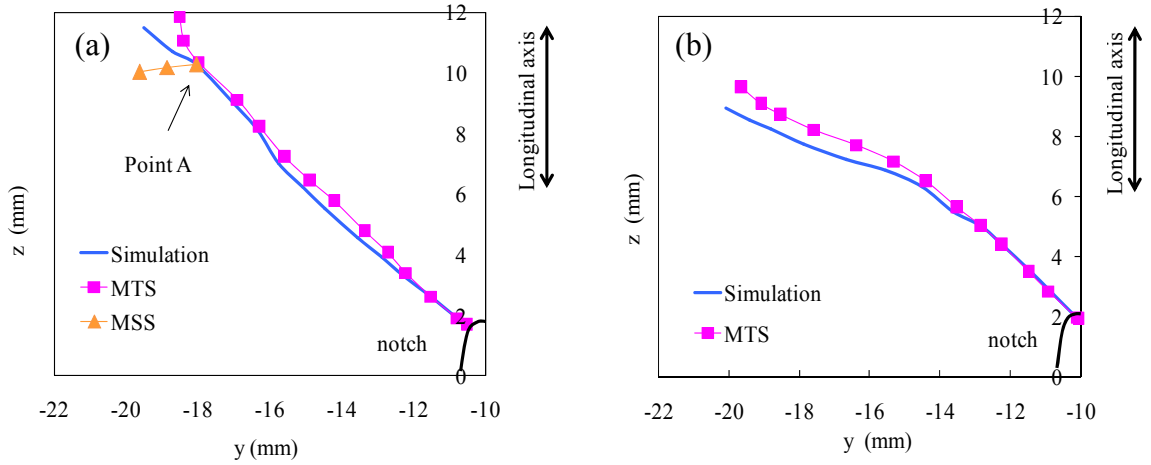

Figure 6. Crack growth path of (a) specimen S13, (b) specimen S7

4.4. Mode transition analysis

The tension mode and shear mode competition under non-proportional mixed mode loading reflects the variation of K_{I} and K_{II} values. Figure 7 illustrates the K_{I} and K_{II} values in one loading cycle under combined tension and torsion with a phase angle of 90°. The equivalent stress intensity factors K_{eq} reaches its peak values $K_{eq,\max}$ at time $t_{\max}$, which is taken as the crack growth driving force. The corresponding K_{I}, K_{II} components are marked as K^*_{I} and K^*_{II}. The K^*_{II} values of each crack propagation step for the four different specimens are shown in Figure 8 (①, ③ represent the corresponding crack paths) based on the calculation results from FRANC3D. The ordinate represents K^*_{II} values (absolute value), the abscissa represents the crack growth step. For all specimens the same tendency of increasing K^*_{II} with crack length is observed. From step 13 for specimen A7, step 15 for specimen A8 and S13, the transition mode started. It can be inferred that a threshold value $K^*_{\mathrm{II\ th}}$ exists in the transition mode. If the mode II component of the maximum equivalent stress intensity factor $K_{eq,\max}$ in a loading cycle, K^*_{II}, is less than the threshold value,

tension mode dominated crack propagation prevails, if a threshold value is exceeded, transition mode dominated crack propagation is a reasonable crack growth pattern. The threshold $K^*_{II\ th}$ is a function of several parameters, such as material property, the R ratio or the mode I threshold value and so on. Further research is needed to complete the concept.

$$K^*_{II} > K^*_{II\ th} \tag{4}$$

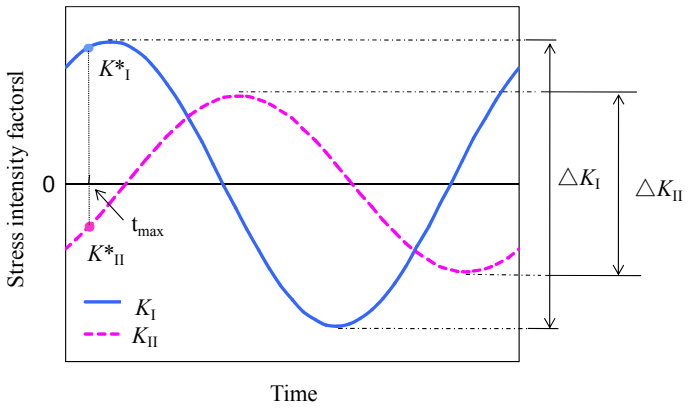

Figure 7. Variation of stress intensity factors

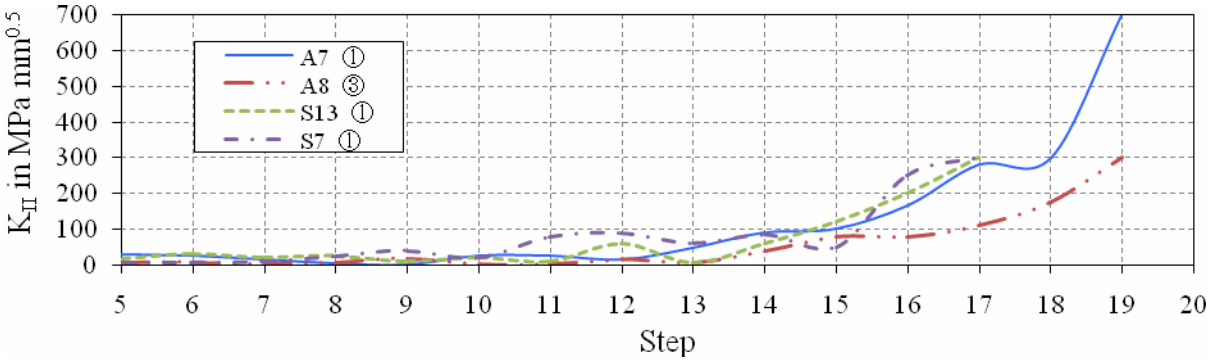

Figure 8. K^*_{II} values

Only for specimen S7 transition and shear modes did not appear. However, the K^*_{II} increased in the same way as for the other specimens. This implies that the crack growth path behaviour is not just controlled by K^*_{II}. Considering one loading cycle, the stress intensity range is defined as: (see Figure 7)

$$\triangle K_i = K_{i\ max}\,(1\text{-}R) \quad (i\text{=I, II}) \tag{5}$$

The ratios of $\triangle K_{II}$ to $\triangle K_I$ in one loading cycle are shown in Figure 9. Similar with K^*_{II} versus crack growth step curve, an ascending tendency is revealed in the ratio of mode II range to mode I range especially for specimen A7 and A8. The transition mode started at step 13 for specimen A7 and at step 15 for specimen A8, the ratio of stress intensity range corresponding to these two steps are larger than 0.4, which could be considered as an assumed threshold value. Although the ratios from step 8 to 11 are also larger than 0.4 in specimen A7, the K^*_{II} values are too small to induce transition mode crack growth. In specimen A7 and A8 shear mode was subsequent from step 18,

step 19, the ratio values are larger than 1.3. It implies that transition mode is not a stable crack growth pattern; a critical ratio of stress intensity factor range is proposed between transition mode and shear mode. Once the proportion of $\triangle K_{II}$ in one loading cycle is large enough, shear mode crack growth occurred.

$$(\triangle K_{II}/\triangle K_I)_{th} < \triangle K_{II}/\triangle K_I < (\triangle K_{II}/\triangle K_I)_{cr} \tag{6}$$

The curves for specimen S13 and S7 are much smoother compared to the curve of A7 and A8. The different loading type may be a main reason to explain this phenomenon. Even so, it can be observed that from step 15 curve S13 increased persistently and the values are larger than 0.25. The curve of S7 does not show a rising trend but a relative downward tendency. It means that the mode I stress intensity range increased faster than the mode II range in this specimen. Transition and shear mode crack propagation is suppressed by this rapidly growing mode I component. The assumed transition mode threshold ratios for specimen A7 and A8, S13 are 0.6, 0.45 and 0.25 respectively. Beside the different material property, plasticity plays an important role in reducing the threshold value for specimen S13. Depending on the loading level, more plasticity compared to A7, A8 is displayed in specimen S13, accelerating the transformation of tension mode to transition mode or even to shear mode.

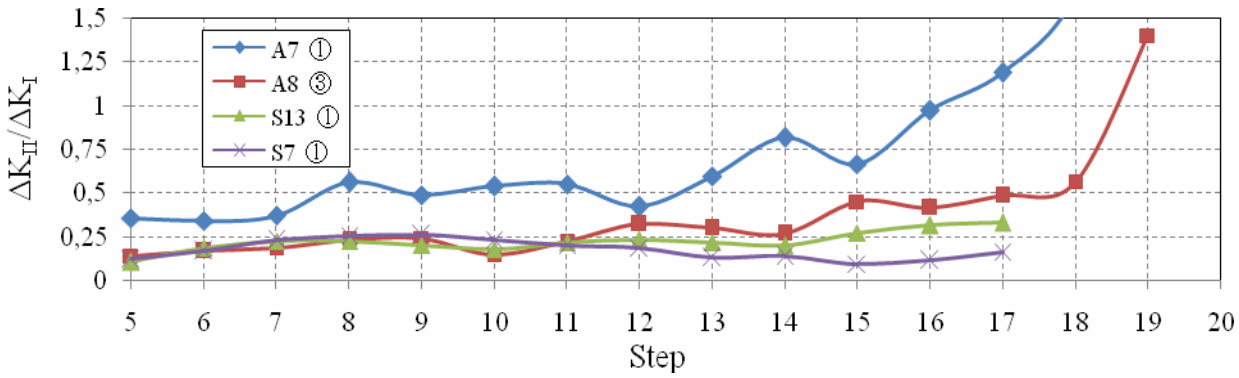

Figure 9. Ratio of stress intensity factors range

5. Conclusions

In the present paper, 3-dimensional crack growth simulation is implemented by using the LEFM-based algorithm. The simulation for two different materials AlMg4.5Mn, S460N, two phase angles 45° and 90°, different loading levels and M_T/F ratio have been presented. The M_T/F ratio has a great influence on the number of cracks, 4 cracks will occur when torsion loading M_T reaches a certain percentage of the total loading. The loading phase angle affects the crack growth path behaviour and also numbers of initiated cracks. Compared to the phase angle of 45°, specimens under out of phase loading with a phase angle of 90°, demonstrate more variations in crack initiation and crack growth path, depending on different load levels and M_T/F ratios.

Under non-proportional mixed mode loading, three distinct features of the crack growth path behaviour are observed which are tension mode, transition mode and shear mode. Based on the

analysis of specimen A7, A8 and S13, crack growth followed tension mode in most cases until the crack reaches a certain length corresponding to:
(1) The mode II component of the maximum equivalent $K_{eq,\max}$ in one loading cycle exceeds a threshold value and in the meantime;
(2) The ratio of mode II stress intensity factor range to mode I stress intensity factor range in one loading cycle is higher than a corresponding threshold value and;
(3) Shear mode crack growth occurs when the latter ratio exceeds a critical value.

Considering that no theoretical hypotheses can be applied to confirm the two threshold values to the transition mode at present, further research is needed to explain the crack growth path behavior under non-proportional loading cases. Further investigations especially in the field of micromechanics may provide more indications for this problem and improve the proposal of the present paper.

Acknowledgements

The authors wish to thank the Senior Research Associate in Cornell Fracture Group, Carter Bruce, for technical advice in FRANC3D operating.

References

[1] Erdogan, F., Sih, G.C., On the Crack Extension in Plates Under Plane Loading and Transverse Shear. J. Basic Engineering, 85D (1963) 519-527.
[2] Sih, G.C., Strain-energy-density factor applied to mixed mode crack problems. Int. J. Fracture, 10 (1974) 305-321.
[3] R. J. Nuismer, An energy release rate criterion for mixed mode fracture. Int. J. Fracture, 11 (1975) 245-250.
[4] Chambers. A. C., Hyde. T. H., Webster. J. J., Mixed mode fatigue crack growth at 550°C under plane stress conditions in Jethete M152. Engng. Frac. Mech, 39 (1991) 603-619.
[5] Hussain, M.A., Pu, S.L., Underwood, J.H., Strain energy release rate for a crack under combined mode I and II. Fracture Analysis, (1974) 2-28. ASTM STP 560, Philadelphia.
[6] Highsmith Jr., S., Crack path determination for non-proportional mixed-mode fatigue. PhD Thesis, Georgia Institute of Technology, USA, (2009).
[7] M. Vormwald, P. Zerres, Review of fatigue crack growth under non-proportional loading. Proceedngs of the 4th international conference on CRACK PATHS, (2012) 1-14.
[8] Y. Yang, M. Vormwald, LEFM-based simulation of fatigue crack growth under non-proportional mixed-mode loading. Proceedngs of the 4th international conference on CRACK PATHS, (2012) 465-472.
[9] Brüning, J., Untersuchungen zum Rissfortschrittsverhalten unter nichtproportionaler Belastung bei elastisch-plastischem Materialverhalten-Experimente und Theorie, Instituts für Stahlbau und Werkstoffmechanik der Technischen Universität Darmstadt, report 85 ISBN 978-3-939195-14-6, Germany. (2008)
[10] D. Haboussa, T. Elguedj, B. Leblé, A. Combescure, Simulation of the shear-tensile mode transition on dynamic crack propagations. Int. J. Fracture, 178 (2012) 195-213.